Guest Forum

Modeling Analysis of Fuel Sprays

Professor
Jiro SENDA
Faculty of Science and
Engineering
Doshisha Unversity
Ph. D

Assistant Professor
Yoshimitsu KOBASHI
Department of Mechanical
Engineering
Kanazawa Institute of
Technology
Ph. D

Current engine development processes in which computations play an important role have sought for numerical models which can accurately represent phenomena in spray combustion. The authors have developed original sub-models taking into account the effects of extensive spray combustion phenomena including nozzle cavitation, droplet breakup behavior, multi-component evaporation process, spray-wall interaction, soot formation and so on. This paper describes authors' models while accompanied by phenomenological descriptions and focusing on how to model the phenomena. In addition, the authors' current work on model development for a model based calibration method is also introduced.

Introduction

Electronic control technology in engine development has advanced dramatically in the recent years, enabling clean and high-efficiency combustion by finding the optimal combination of many control variables of various electronic devices. However, the control variables continue to grow in number as they need to comply with the fuel consumption regulations and exhaust gas regulations which are ever stricter. Of these variables, many development man-hours are required for common rail-type fuel injection systems with high freedom in injection pressure, injection count and timing as well as for diesel engines equipped with Exhaust Gas Recirculation (EGR), superchargers and so forth, making it difficult to experimentally determine all the optimal settings for control variables within the limited time and resources the engine manufacturers have.

Meanwhile, engine development utilizing model-based methods has gained popularity these days, and the manufacturers are adopting various different measures in order to improve the efficiency in engine development which continues to be more complicated and increase in scale[1-3]. However, in the combustion chamber of an engine whose trunk power source is nonsteady spray combustion (such as that of a diesel engine for automobiles), liquid or air-liquid multiphase flow running faster than 500 m/s passes through a nozzle with hole diameter around 0.1 mm to be injected, atomized, mixed with air, evaporate, ignite and combust through interference with the wall boundary within only several milliseconds. Numerical modeling of such small-scale, high-speed phenomena which are complex both physically and chemically is still being developed, and construction of a model that can capture the phenomena precisely as

Table 1 History of the authors' models

1981	Wall-impingement analysis based on SMAC method
1983	Analysis of cavitation bubbles behavior under oscillation pressure
1990	Diesel fuel injection system analysis with taking into account cavitation effects
1993-	Spray-wall interaction model
1993	Modeling of sprays accompanied by flash boiling (0-dimensional)
1993-	Vapor-liquid equilibrium model for multi-component fuels (0-dimensional)
1996	Modified TAB droplet breakup model
2000-	Multi-component fuel evaporation model (multi-dimensional)
2001	Spray-wall interaction model available for multi-component fuel
2002	Integrated version of spray-wall interaction model
2002-	Kinetic modeling of soot formation with detailed chemistry
2003-	KIVA simulation coupled with CHEMKIN and soot model
2004-	Modeling of sprays accompanied by flash boiling (multi-dimensional)
2005-	Large eddy simulation of diesel sprays
2006-	Cavitation-induced droplet breakup model
2006-	Phenomenological 1-D multi-component spray model

well as improvement in calculation accuracy are demanded. Under such circumstances, the authors have worked on relatively detailed numerical modeling of various processes in spray combustion. Table 1 shows the list of these models. They vary from the effect of cavitation bubbles formed inside the nozzle to the mode of liquid droplet atomization, multicomponent fuel droplet vaporization process, spray-wall interaction, and generation of soot based on various chemical reactions. In this article, the main points of each model will be described along with the phenomenological background. In addition, development of a Model Based Calibration (MBC) model, on which the authors are currently working, will be described at the end of the article.

Modeling Related to Fuel Spray Atomization

Atomization of liquid droplets in engine spray is a phenomenon which is affected by turbulence or cavitation occurring inside the nozzle and which is smaller in scale than general computational grids. Therefore, modeling of this phenomenon requires a link to the flow inside the nozzle as well as proper description of the atomization mechanism. This chapter thus describes several droplet

breakup models constructed with consideration of these.

Liquid droplet breakup model with consideration of cavitation in nozzle

The fuel liquid flowing into the fuel injection nozzle orifice at a high speed forms a low-pressure field during contraction, and generates cavitation bubbles. While it is known that these bubbles affect the atomization of spray[4], it is not easy to elucidate the entire picture of this minute and ultrafast phenomenon which also contains many bubbles. The authors therefore focused on a phenomenon that occurs when the generated cavitation bubbles are exposed to the high pressure downstream in the nozzle, which is the shock wave generated when they collapse at a contraction rate high enough in some cases to exceed the sound of speed. This shock wave is large enough to cause erosion in metallic materials[5]. We developed a model that connects the energy generated in these processes with breakup of spray liquid droplets[6]. Figure 1 shows an outline of the model. The history of cavitation bubble growth and contraction is solved using the Rayleigh-Plesset equation and the kinetic energy E_{shrink} for the surrounding fluid induced when the bubbles contract rapidly is calculated using the following equation:

$$E_{shrink} = 1/2\, \rho_l \sum_{R_0} N(R_0) \int_{r=R_{i+1}}^{r=R_i} \dot{R}^2 \cdot 4\ r^2 dr\pi \quad \cdots\cdots \text{(1)}$$

(ρ_l: Liquid density, R: bubble radius, N: number of bubbles with initial radius R_0)

In addition, the maximum shock wave pressure[5] p_{max} when bubbles collapse is calculated as

Primary breakup based on Kelvin-Helmholtz instability
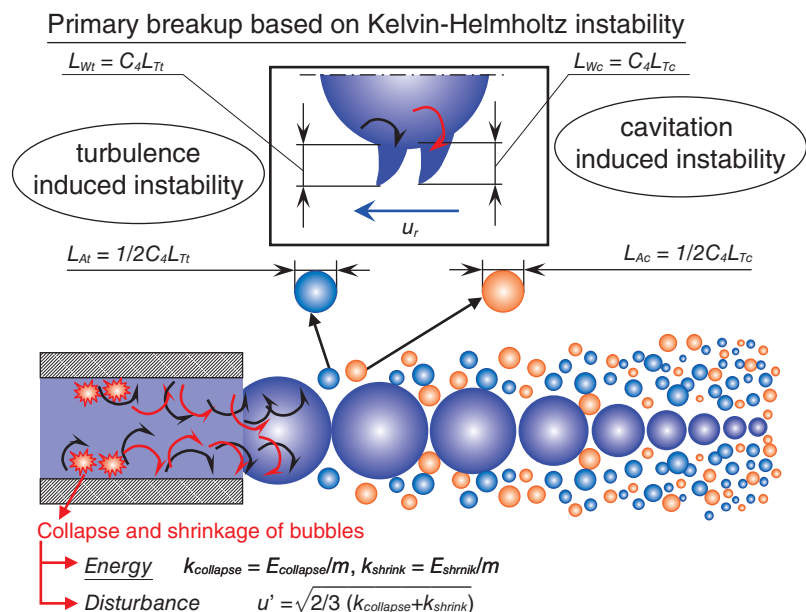

Figure 1 Conceptual diagram of cavitation-induced breakup model
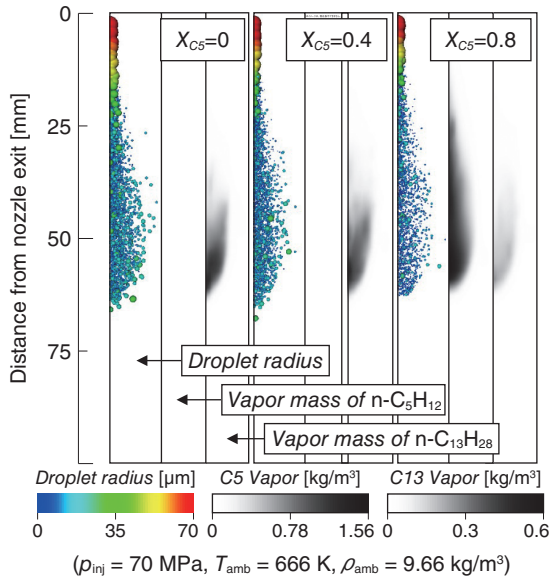
Figure 2   Spray images of binary fuel blends consisting of n-C5H12 and n-C13H28, predicted by cavitation-induced breakup model

$$p_{max} = p_{gRmax} (R_{max}/R_{brk})^{3n} - 2\sigma/R_{brk} \quad \cdots\cdots\cdots\cdots (2)$$

(p_{gRmax}, R_{max}: Pressure inside the bubble and bubble radius when a bubble reaches its maximum diameter, R_{brk}: bubble radius at collapsing, σ: surface tension)

And its energy $E_{collapse}$ is expressed as follows:

$$E_{collapse} = 4\pi/3 \sum_{R_0} N(R_0) \cdot p_{max}(R_0) \cdot R^3_{brk} \quad \cdots\cdots (3)$$

When they are converted into dynamic energy k_{shrink} and k_{shrink}, respectively by dividing these with the injected mass per time step m, the turbulence fluctuation element u' for nozzle outlet is determined based on supposition of isotropic turbulence.

$$u' = \sqrt{2/3 (k_{collapse} + k_{shrink})} \quad \cdots\cdots\cdots\cdots\cdots\cdots (4)$$

It is supposed that the turbulence fluctuation u' at nozzle outlet helps the Kelvin - Helmholtz instability on jet

surface in a similar fashion to the model by Huh and Gosman[7]. Defining the length scale for atomization deriving from the size of the surface wave for this jet as L_A and the sum of the time scale for turbulence ascribed to turbulence fluctuation u' and time scale for surface wave as time scale for atomization τ, the rate of change in liquid droplet radius r_d is expressed by the following equation:

$$dr_d/dt = -CL_A/\tau \qquad C: \text{Constant} \quad \cdots\cdots\cdots (5)$$

As an example of calculation results, diesel spray mixing n-tridecane (n-$C_{13}H_{28}$) with n-pentane (n-C_5H_{12}) and changing the mixture rate X_{C5} is shown in Figure 2. It shows that the cavitation bubbles in injection hole grow larger as the amount of n-C_5H_{12} with a high saturated vapor pressure that is mixed is larger, resulting in rapid atomization and expansion from near the injection hole with the energy in Equation 1 and Equation 3 growing.

Improvement in TAB model and hybrid liquid droplet breakup model

Besides the above model, many droplet breakup models have been proposed in the past. The KIVA code used in numerical calculation of engine combustion uses the Taylor Analogy Breakup (TAB) model[8] by O'Rouke, et al. in droplet breakup model for its version II and later. TAB model considers the liquid droplet as an elliptical oscillating body and applies a spring-mass system model for its deformation, and the droplet radius after breakup is given as the X^2 distribution with Sauter average particle size r_{32} indicated by the following formula:

$$r_{32} = r \left/ \left(1 + \frac{8K}{20} + \frac{6K-5}{120} \frac{\rho_l r^3}{\sigma} \dot{y}^2 \right) \right. \quad \cdots\cdots\cdots\cdots (6)$$

However, model constant was set as $K=10/3$ and degree of freedom in X^2 distribution $ø=2$ in the original paper. Here, Figure 3 shows the distribution of particle size compared to the degree of freedom $ø$. In X^2 distribution with degree
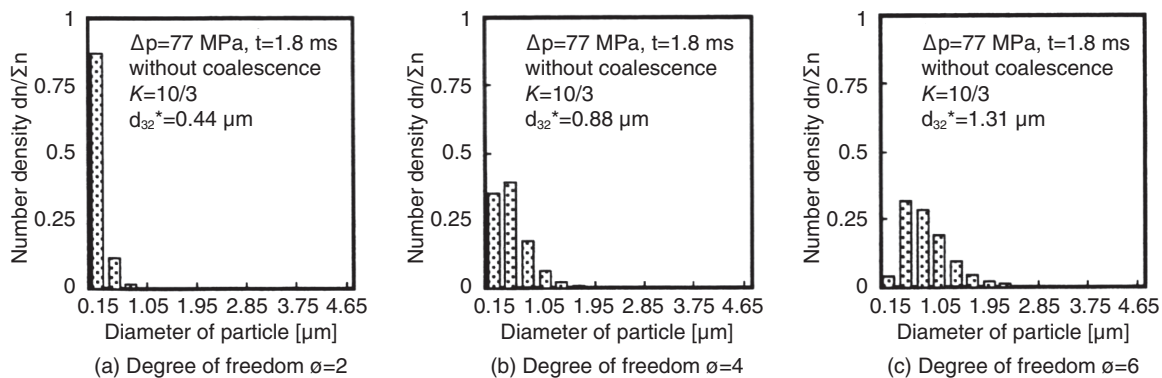

Figure 3   Comparison of particle size distribution between the degrees of freedom

of freedom ø=2, the particle size distribution is to inclined toward small diameter side. Compared to this, the authors proposed that the corrected TAB model with degree of freedom being ø=6 and model constant K=0.89 reproduced the particle diameter distribution in diesel spray favorably[9].

Meanwhile, the mode of breakup in TAB model has similar characteristics to those of breakup with low Weber number ($We=\rho_g r_d v_{rel}^2/\sigma$, ρ_g: gas density, r_d: liquid droplet radius, v_{rel}: relative velocity, σ: surface tension)[10]. While such a form of breakup is observed at a position away from the injection hole of pressure injection valve in general, it is considered that the instability of surface wave and so forth dominantly contribute to atomization in regions with high Weber numbers near the injection hole. That is, several liquid droplet breakup model need to be combined for numerical analysis of fuel injection involving various atomization mechanisms. Considering this point, the authors once used the KH-RT model combining the Kelvin-Helmholtz instability (primary breakup) and Rayleigh-Taylor instability (secondary breakup)[11], and a model combining the above modified TAB (MTAB) model, Kelvin-Helmholtz instability (WAVE model[12], primary breakup) and MTAB (secondary breakup) to verify the validity of liquid droplet breakup model in Large Eddy Simulation (LES) for diesel spray[13]. Here, the concept of LES is shown in Figure 4. Unlike Reynolds Averaged Navier-Stokes (RANS) which solves the averaged Navier-Stokes equation, LES models only the high-frequency component of turbulence and

directly solves the anisotropic, low-frequency component with high dependency on the flow field. It is a solution method expected to solve the turbulence behavior with higher precision than RANS, which models and solves all eddy components.

Figure 5 compares the spray images for the numerical calculation and experiment results. Since calculation using LES calculates relatively large eddy structures that cannot be expressed by RANS[14], sprays with branch-like structures that can be seen in experiments are calculated.
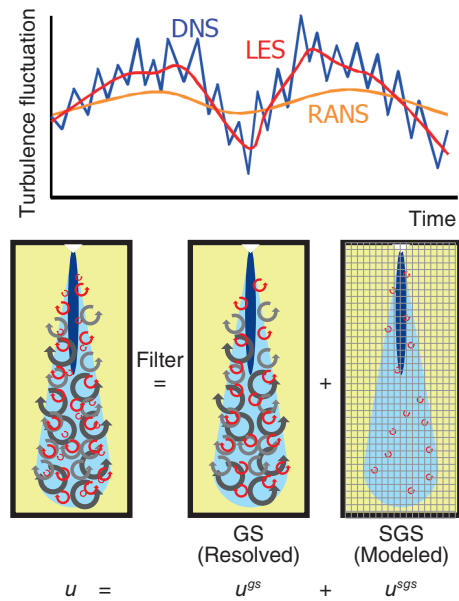

Figure 4   Schematic images of LES of diesel spray

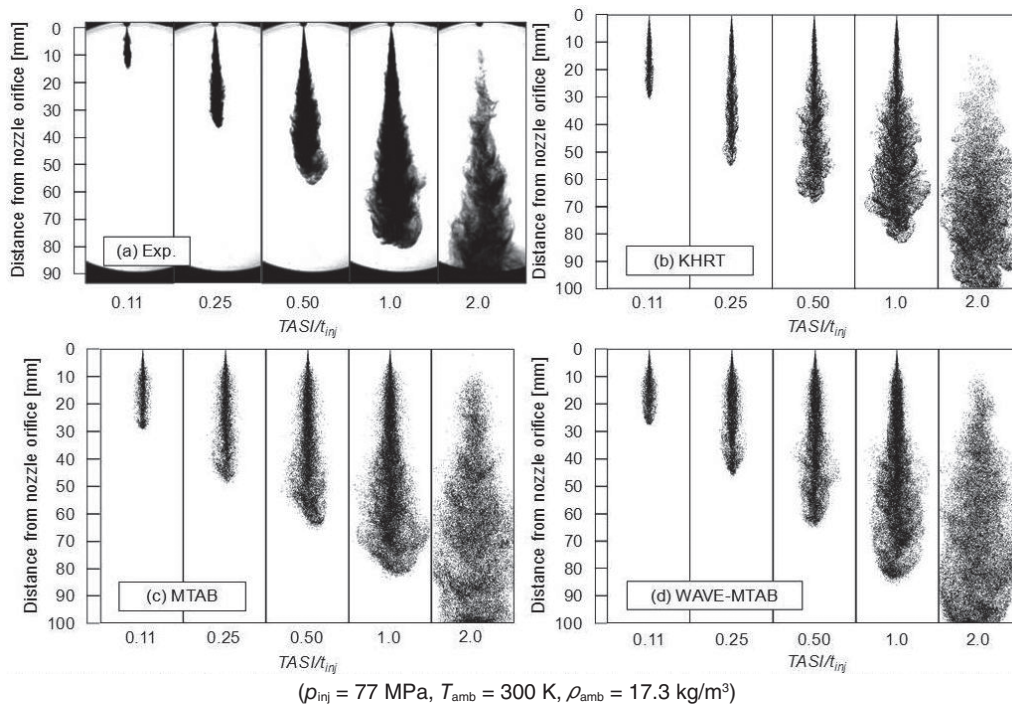(p_{inj} = 77 MPa, T_{amb} = 300 K, ρ_{amb} = 17.3 kg/m³)

Figure 5   Change in spray structure calculated by large eddy simulation with breakup models
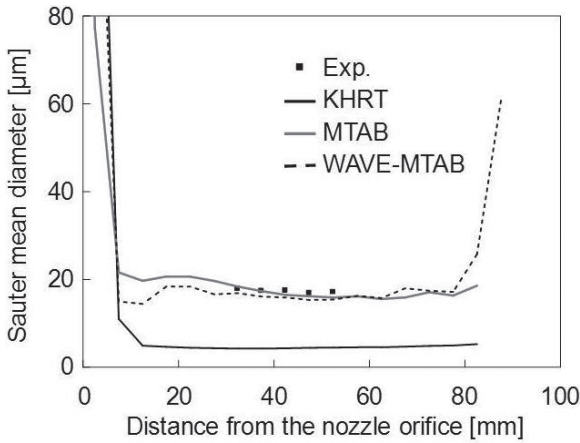
Figure 6   Effect of droplet breakup model on Sauter mean diameter distribution using LES

Figure 7   Change in shape of n-pentane spray as a function of ambient pressure

Here, **Figure 6** indicates the distribution of Sauter's mean diameters. As KH-RT underestimates the liquid droplet diameter after breakup, the liquid droplets after breakup follow the eddy motion of the surrounding gas too excessively as a consequence. On the other hand, Sauter's mean diameters by MTAB model and WAVE-MTAB model generally match the experimental values. It was shown that WAVE-MTAB model in particular reproduced the spreading of the spray observed in experiments more faithfully than MTAB model.

Modeling of flash boiling spray

While the cavitation in the nozzle as described previously is a phenomenon in which the generated bubbles collapse under the pressure downstream, flash boiling occurs in which the bubbles continue to grow, although it concur with rapid vaporization, when the saturated vapor pressure of the fuel is high and the fuel is injected into a field with low pressure such as the engine suction pipe. **Figure 7** shows the spray image when n-C_5H_{12} is injected into atmosphere with different atmospheric pressure p_b
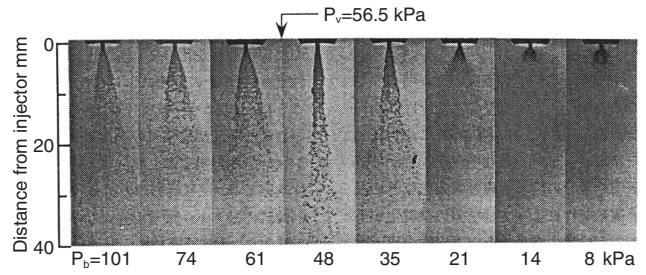
values. The saturated vapor pressure of n-C_5H_{12} is 56.5 kPa. When p_b is set to a lower value, the spray becomes narrower once but then expands rapidly and goes through flash boiling which forms fine liquid droplets. The authors have worked on development of a model that can describe these characteristics of flash boiling. **Figure 8** shows an outline of a flash boiling model developed on liquid film ejected from a pintle-type nozzle[15]. The number of bubble nuclei N with radius R generated at the nozzle orifice is calculated by the following theory of nucleation:

$$N = C \cdot \exp\left(\frac{-\Delta A}{k\Delta\theta}\right), \Delta A = \frac{4}{3}\pi R^2 \cdot \sigma \quad \cdots\cdots (7)$$

(C: Constant, k: Boltzmann's constant, $\Delta\theta$: degree of superheat for liquid)

Similarly to the prior cavitation model, the changes in radii of the generated bubbles in time are calculated by supposing that they grow according to the Rayleigh-Plesset equation (however, a term for surface viscosity has been added) as indicated in the figure. Using the void fraction defined by the ratio between bubble phase volume V_{bubble} and liquid volume V_{liquid},

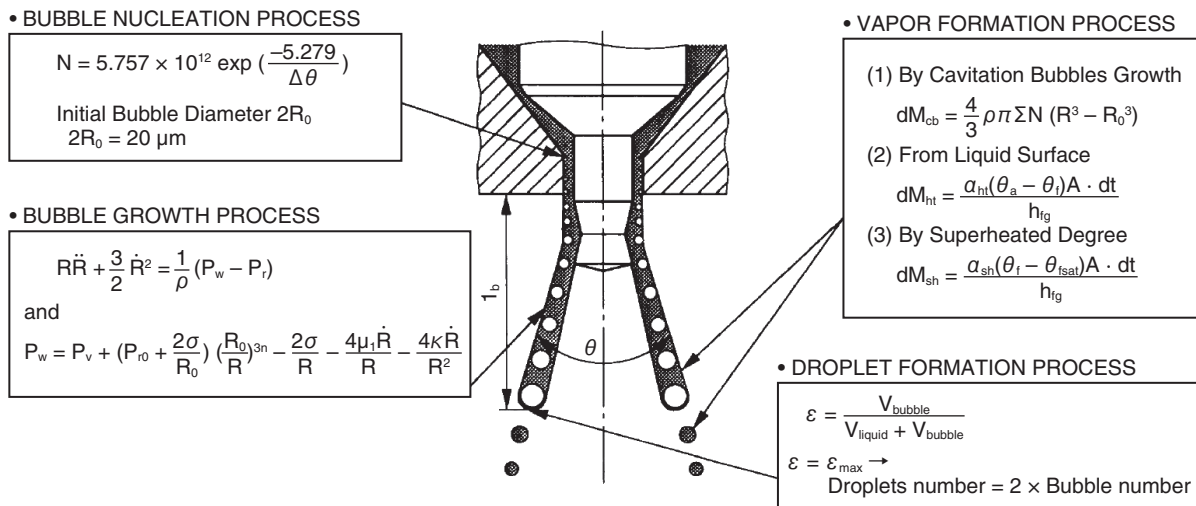$$\varepsilon = V_{bubble} / (V_{bubble} + V_{liquid}) \quad \cdots\cdots\cdots (8)$$

Figure 8   Conceptual diagram of flashing spray model, applied to pintle-type nozzle
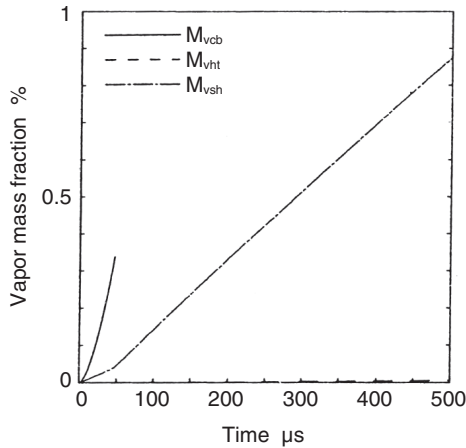
Figure 9　Comparison of n-pentane vapor mass fractions due to bubble growth, M_{vcb}, heat transfer, M_{vht}, and degree of superheat, M_{vsh}, at ambient pressure of 14 kPa

as the criteria, liquid film breakup is modeled by the following equation which links the number of droplets after breakup n_d and the number of bubbles n_{bub} as soon as it exceeds the certain critical void fraction ε_{crit}:

$$n_d = 2 \times n_{bub} \quad\cdots\cdots\cdots\cdots\cdots\cdots\cdots\cdots\cdots\cdots\cdots (9)$$

Meanwhile, flash boiling is an instantaneous phase change phenomenon for superheated liquid subjected to pressure reduction to lower than the saturated vapor pressure, and its form is different from that of heated boiling by heat transfer. Phase change during flash boiling is classified into evaporation in concurrence with cavitation bubble growth M_{vcb}, evaporation caused by heat

transfer from droplet surface M_{vht}, and evaporation caused by the degree of superheating M_{vsh}, and the rate equation for each is shown in **Figure 8**. **Figure 9** shows a comparison of vapor mass fractions originating in each evaporation process after injecting n-C_5H_{12} at 14 kPa back pressure. It is evident that evaporation by cavitation bubbles M_{vcb} is larger than that of other types. Although evaporation caused by the degree of superheating M_{vsh} is sufficiently large compared to one caused by heat transfer M_{vht}, its amount of evaporation is not as large as that of M_{vcb}, it was shown that vapor formation by bubble growth was dominant in flash boiling spray.

Modeling on Evaporation of Multi-Component Fuel Spray

Most commercial fuels distributed on the market such as gas oil and gasoline are multi-component mixtures, but are handled as pseudo-single-component material comprising of those with similar properties in spray combustion numerical analysis. However, it is becoming impossible to neglect the multi-component properties of fuels due to the recent sophistication and advances in engine combustion control technology, advances in fuel diversification including mixed use of biomass fuels and so forth. This section will describe the evaporation characteristics in which consideration of multi-component properties is important, and show their typical examples. **Figure 10** shows the distillation curve for a mixture of 10 components with the boiling points of individual single
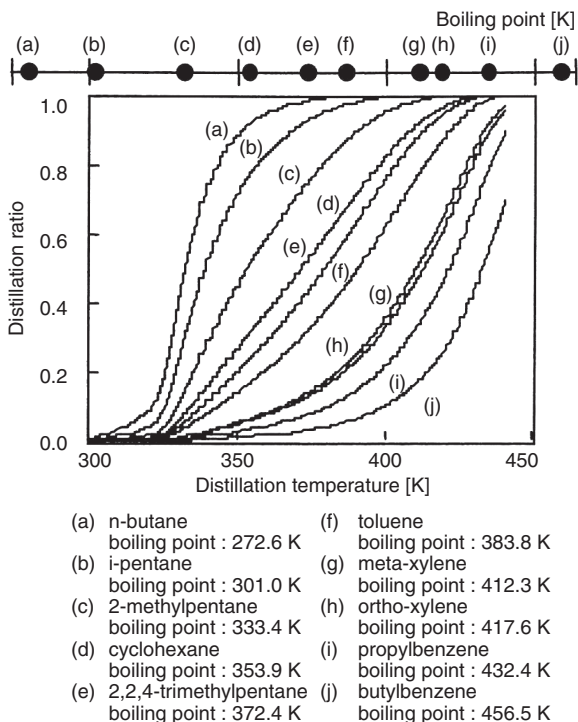

(a) n-butane
　　boiling point : 272.6 K
(b) i-pentane
　　boiling point : 301.0 K
(c) 2-methylpentane
　　boiling point : 333.4 K
(d) cyclohexane
　　boiling point : 353.9 K
(e) 2,2,4-trimethylpentane
　　boiling point : 372.4 K
(f) toluene
　　boiling point : 383.8 K
(g) meta-xylene
　　boiling point : 412.3 K
(h) ortho-xylene
　　boiling point : 417.6 K
(i) propylbenzene
　　boiling point : 432.4 K
(j) butylbenzene
　　boiling point : 456.5 K

Figure 10　Distillation characteristic of multi-component blend
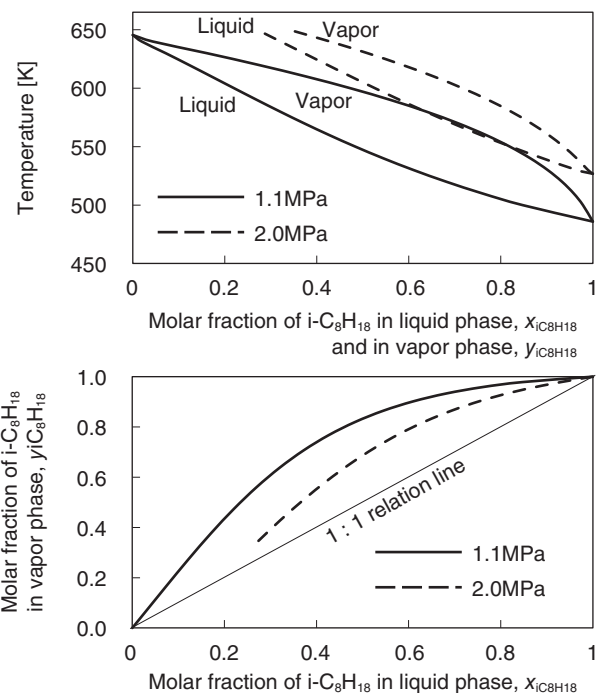
Figure 11　*T-xy* and *x-y* diagrams of i-C_8H_{18}/n-$C_{13}H_{28}$ blends at constant pressure
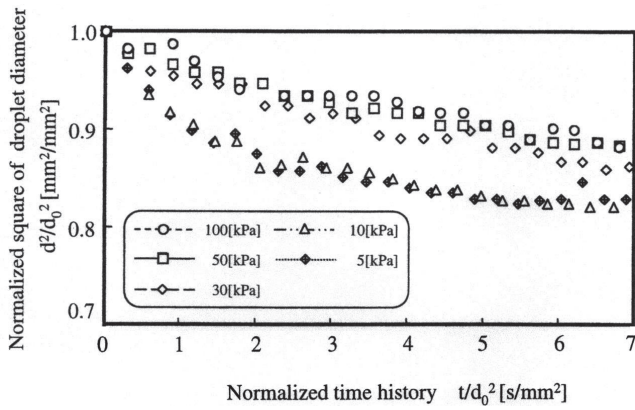
Figure 12   Temporal change in square of single droplet diameter of n-C_6H_{14}/n-$C_{13}H_{28}$ blend

components indicated on top. Unlike the single components, the components of the mixture do not show clear boiling point but evaporate with certain gradient toward the distillation temperature. In addition, the distillation temperature for low-boiling point components relatively rise and that for high-boiling point components relatively decrease, making the distillation temperature range narrower than the range of boiling points for individual components. Figure 11 shows the constant-pressure vapor-liquid equilibrium for i-C_8H_{18} and n-$C_{13}H_{28}$ (T-xy, x-y diagram). When we focus on x-y diagram, the rate of i-C_8H_{18} in gas phase composition is higher than in liquid phase composition. This indicates the possibility that i-C_8H_{18} with a lower boiling point forms more vapor even in droplet evaporation process. Figure 12 shows the evaporation process for a single droplet of a mixed fuel (molar fraction 5:5) comprising of n-C_6H_{14} and n-$C_{13}H_{28}$ in a field with rapidly decreasing pressure. In general, evaporation of a single droplet follows the so-called d^2 rule, in which the square value of droplet diameter relatively becomes smaller in time. However, as it is considerable at low pressure, the d^2 value for a mixed fuel drops considerably in the beginning and continues to decrease slowly. This is because the low-boiling point component n-C_6H_{14} evaporates in a large amount in the beginning and n-$C_{13}H_{28}$ remaining in the droplet evaporates relatively later.

As it is expected that such evaporation characteristics of multi-component fuels would affect the later ignition and combustion characteristics, the authors have been working on modeling this phenomenon. More specifically, a method using detailed vapor-liquid equilibrium calculation by incorporating commercial source code SUPERTRAPP[17] by the U.S. NIST into KIVA3V[16] was adopted[18]. In nonideal solutions with molecules of different sizes, the vapor-liquid equilibrium condition is expressed by the equation below:

$$\phi_i^V y_i p = \phi_i^L x_i p \qquad (10)$$

(ϕ_i: Fugacity coefficient, V: vapor phase, L: liquid phase, x_i: molar fraction of component i in liquid phase, y_i: molar fraction of component i in vapor phase, p: total pressure)

Therefore, it is possible to calculate the equilibrium concentration between vapor and liquid phases by calculating the fugacity coefficient using a state equation for mixtures applicable to both vapor and liquid phases (Peng–Robinson equation of state in the model by the authors). A modified Spalding model[19] is used for the droplet evaporation model. The heat transfer rate $\dot{Q}$ to the droplet and mass transfer rate $\dot{m}$ from the droplet are expressed as follows:

$$\dot{Q} = 2\pi r \lambda_s (T_\infty - T_d) Nu \qquad (11)$$

$$\dot{m} = 2\pi r \rho D_{air} B_M Sh \qquad (12)$$

(r: Droplet radius, λ_s: heat transfer coefficient, T_∞: ambient temperature, T_d: droplet temperature, ρ: liquid density, D_{air}: diffusion coefficient for fuel in air)

In addition, Spalding's mass transfer number B_M is calculated as follows:

$$B_M = \left(\sum y_{i,s} - \sum y_{i,\infty} \right) / \left(1 - \sum y_{i,s} \right) \qquad (13)$$

(y_i: Mass fraction for component i, s: droplet surface, ∞: infinity)

The above vapor-liquid equilibrium computation is used here. Equilibrium composition for the vapor phase is calculated for the mixture of fuel components and nitrogen (atmosphere gas) to calculate $y_{i,s}$. In addition, Equation 11 and Equation 12 are calculated using the following formulae:

$$Nu = [2.0 + 0.6Re^{1/2}Pr^{1/3}] / (1 + B_T)^{0.7} \qquad (14)$$

$$Sh = [2.0 + 0.6Re^{1/2}Sc^{1/3}] / (1 + B_M)^{0.7} \qquad (15)$$

$$B_T = C_p (T_\infty - T_s) / Q \qquad (16)$$

(Re: Reynolds number, Pr: Prandtl number, Sc: Schmidt number, B_T: Spalding's heat transfer number, C_p: heat capacity, Q is the quantity of heat reaching the droplet per unit mass until vapor is formed)

Figure 13 shows the distribution of vapor concentration in spray and flame temperature for a fuel mixing i-C_8H_{18} (iC8, 372 K boiling point, 12 cetane number), i-$C_{16}H_{34}$ (iC16, 520 K boiling point, 15 cetane number) and

Shadow (Exp.)	Comp. No.1	C13	OH radical (Exp.)	Temp.

C13: t_{inj}=0.65 ms   0.70 ms   0.65 ms   0.80 ms

iC8/C13: t_{inj}=1.34 ms   1.25 ms   1.34 ms   1.35 ms

C16/C13: t_{inj}=1.26 ms   1.35 ms   1.26 ms   1.45 ms

Vapor density [kg/m³]
0   1.0   2.0

Temperature [K]
900   1800   2700

(p_{inj} = 70 MPa, T_{amb} = 940 K, ρ_{amb} = 16.2 kg/m³)
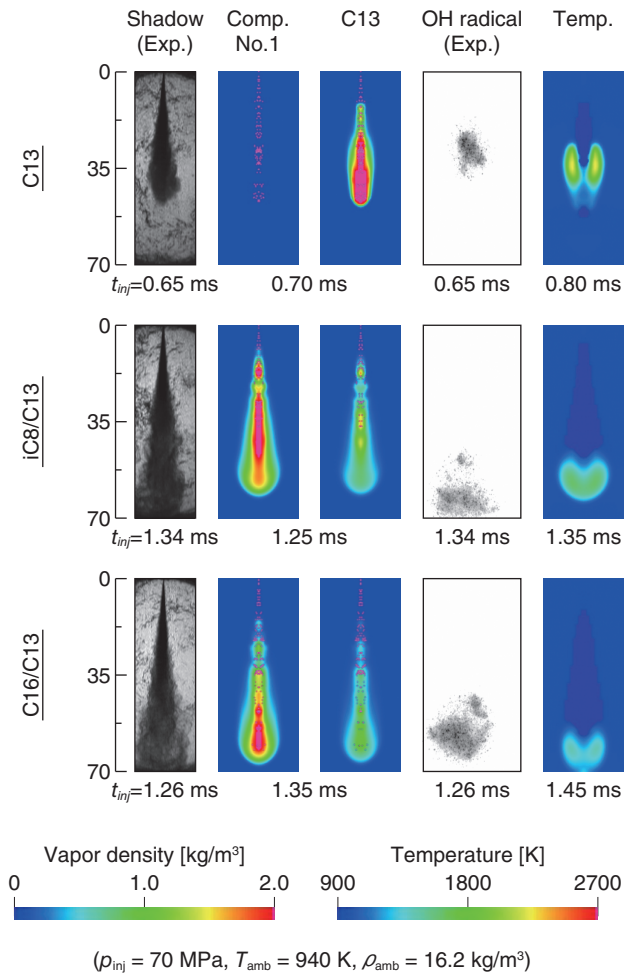
Figure 13   Distributions of fuel vapor and temperature, calculated by multi-component fuel model

n-$C_{13}H_{28}$ (C13, 510 K boiling point, 88 cetane number) at mass fraction of 0.69 each[20]. The process of ignition and combustion was modeled by combination of Shell model[21] and one-step overall reaction. It favorably expressed the experimental results including ignition delay when i-C_8H_{18} or i-$C_{16}H_{34}$ was mixed, reaching distance for spray edge and combustion area in this case. It also enabled analysis that could express the evaporation characteristics of blended fuels such as evaporation of i-C_8H_{18} beginning from the upper stream and decrease in quantity of n-$C_{13}H_{28}$ evaporation when i-$C_{16}H_{34}$ was mixed.

Modeling of Spray-Wall Interaction

It is important to know the behavior of liquid droplets and films when fuel spray impinges on the wall surface and the process of the later fuel diffusion in spray combustion which occurs in the finite space of an engine. The authors have so far constructed systematic models that covered a wide range of phenomena including wall impingement of spray droplets to liquid film formation, splash breakup, liquid film flow and evaporation. As we do not have enough space to describe everything, an outline of each model is provided in this section while leaving the details to the literature.

Low-temperature wall surface model and high-temperature wall surface model

To construct a model that can adapt to both non-evaporation spray impingement corresponding to cold start and spray impinging on a high-temperature wall in evaporation field corresponding to high-load operation, we first modeled the relationship between these two by defining the wall surface temperature as T_w and the saturated temperature for fuel droplet as T_{sat} and distinguishing them into T_w<T_{sat} and T_w≧T_{sat}. Figure 14 shows its overview. The liquid film formation process was

Nozzle

Impinging spray

T_l

Wall T_w

T_{sat} : liquid saturated temperature

T_l : temperature of impinging droplet

T_w : wall temperature

I $T_w < T_{sat}$

(i) Model on fuel film formation on wall

(ii) Model on fuel film breakup due to impinging droplet after film formation
· Assumption on breakup droplets diameter and breakup volume

(iii) Consider jet model by Naber-Reitz concerning dispersing droplet velocity

II $T_w ≧ T_{sat}$

(i) Model on breakup of impinging droplet due to boiling phenomena at liquid-solid interface
· Assumption on breakup droplets diameter

(ii) Model on heat transfer from wall to impinging droplet
· $Q = a \cdot S \cdot \tau \cdot (T_w - T_l)$
· Assumption on droplet contact area S and residence time τ on wall

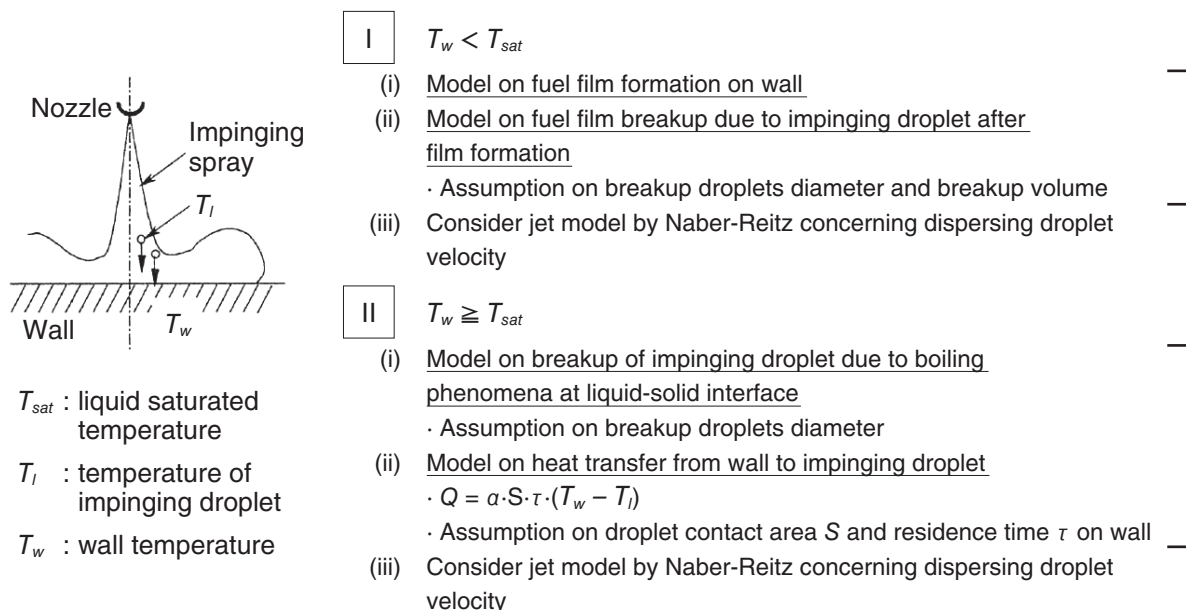(iii) Consider jet model by Naber-Reitz concerning dispersing droplet velocity

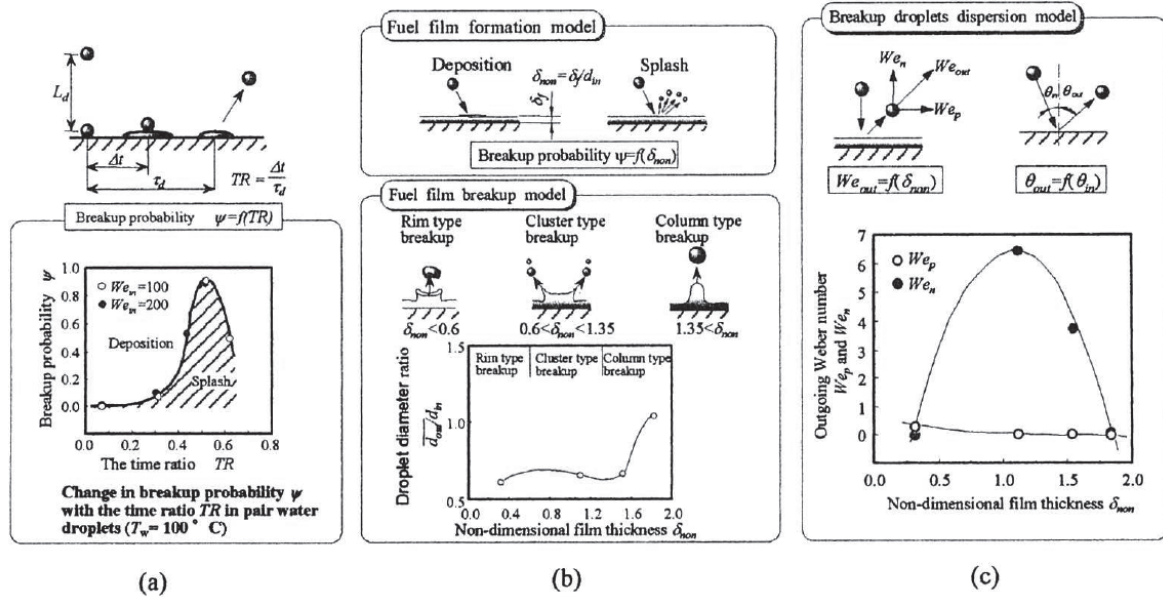Figure 14   Overview of low/high temperature model

Figure 15   Impingement model for low Weber number ($We \leqq 300$)

modeled for low-temperature wall surface ($T_w < T_{sat}$) as liquid droplets would adhere and accumulate on wall surface as well as the liquid film splash breakup in concurrence with droplet impingement after pool-like liquid film formation. For high-temperature wall surface ($T_w \geqq T_{sat}$), breakup process with consideration of heat transfer between droplets and wall surface, and boiling phenomenon between impinging droplets and high-temperature wall surface[22, 23]. Please see Literature [24], [25] for details about the above model.

Liquid film formation model

The authors further focused on the phenomenon in which fuel spray impinging on wall surface, and modeled it with consideration of breakup/diffusion phenomenon caused by droplet-wall interaction, interference effect among droplets, liquid film formation process. In this case, the energy of the impinging droplet or Weber number defined by $We = \rho_1 dv^2 / \sigma$ (ρ_1: liquid density, d: incident droplet diameter, v: incident droplet velocity, σ: surface tension) was used to evaluate and classify into cases with low energy ($We \leqq 300$, Figure 15) and those with high energy ($We > 300$, Figure 16). Modeling for low impingement energy was conducted with consideration of the effects of interactions between droplets or between droplets and liquid film when droplets impinge continuously. In addition, modeling for high impingement energy was conducted with focus on the Splash phenomenon by impingement of droplets against wall surface. The wall surface impingement behavior varies depending on the
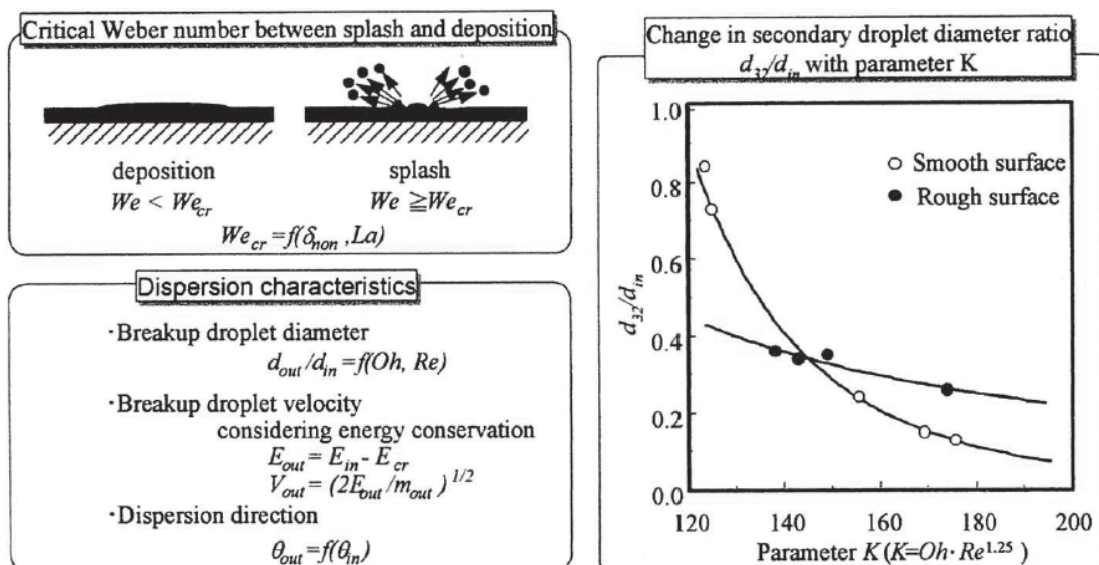

Figure 16   Impingement model for high Weber number ($We > 300$)

existence of liquid film on wall surface during impingement in each case. The mode of breakup for impinging droplets can be expressed by using the dimensionless film thickness for liquid film and the Weber number for droplets when liquid film is formed on the wall surface[29, 30]. For dry wall surface, interactions between droplets were considered when the impingement energy was low and droplet Splash phenomenon was considered using the critical Weber number when the impingement energy was high.

The thickness of liquid film adhering to the wall surface as shown here is important in determining the mode of breakup and dispersion. Thus authors conducted modeling of liquid film expansion in liquid film formation process by considering that the sum of the initial kinetic energy of a droplet and the energy of surface tension is equal to the sum of the energy by surface tension for the maximum diameter of the liquid film and the energy loss by friction. Furthermore, the thickness of the film formed by impingement of a droplet has the same temperature as the droplet initially and then the heat quantity given from the wall surface or ambient gas is expended in its temperature increase and evaporation. Therefore by considering that the heat quantity supplied to the liquid film equals to the heat quantity consumed by the liquid film, the amount of liquid film evaporation was calculated based on the law of energy conservation. Figure 17 shows a comparison of the spatial distribution of fuel vapor and droplet parcels at time 1.4 ms after injection start with injection pressure 99 MPa and impingement distance 30 mm with the vapor phase and liquid phase at the same time shot by Exciplex fluorescence method. (a) in the figure shows the Exciplex fluorescence image, (b) the KIVA-II original code, (c) the Naber-Reitz model[31], and (d) a model by the authors. It is evident that (b) has low fuel vapor concentration and small upward expansion on the wall, that (c) had large-diameter droplets adhering to the upper wall surface at the tip of the spray with slow evaporation, and that the model by the authors in (d) expressed characteristics relatively closer to the experiment results.

Liquid film flow model

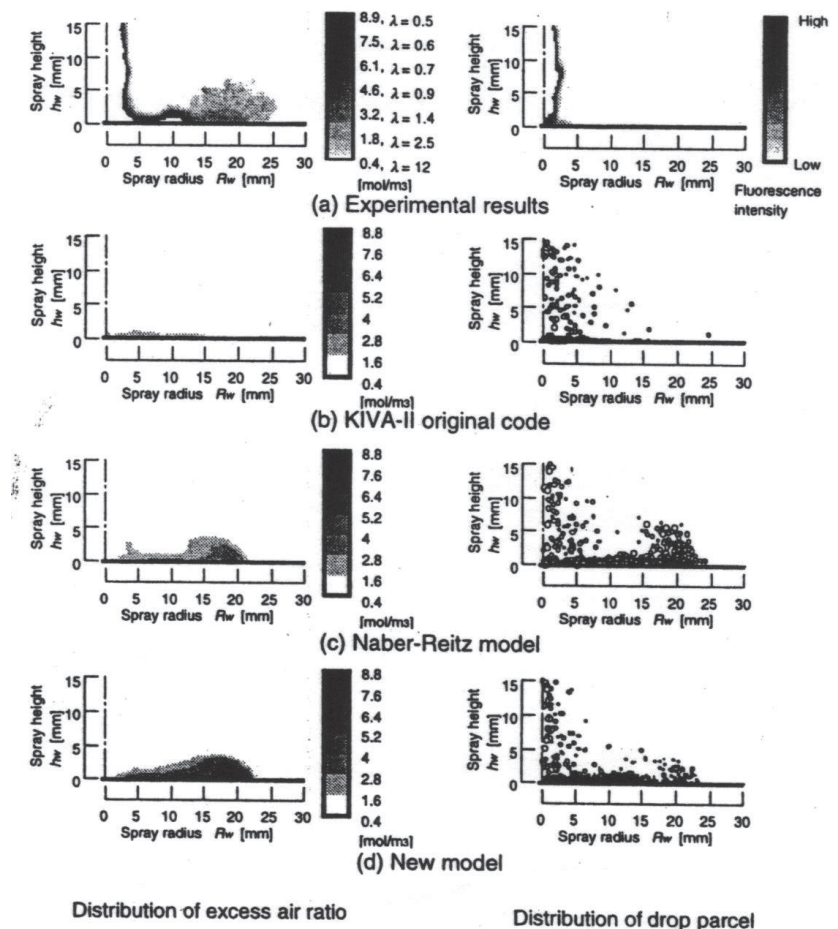The above model cannot describe the behavior of

Figure 17   Comparison of spatial distribution of fuel vapor concentration and droplets between experiment and impingement models

impinging droplets which is affected by film thickness as it has liquid film adhering to the wall surface saved for each cell and does not consider its flow. Therefore, the authors added the liquid film flow model shown in Figure 18 to calculate the liquid film movement velocity by solving an equation of motion which takes into consideration the three factors: momentum of incident
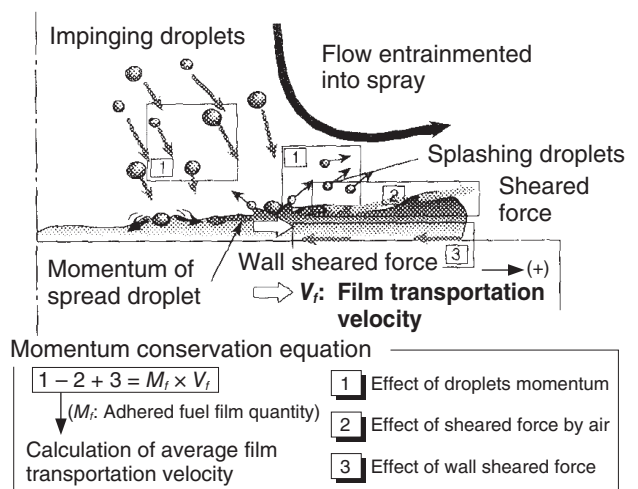

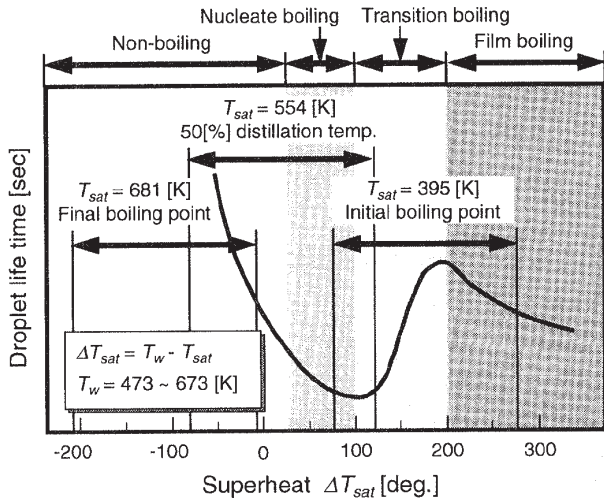Figure 18   Physical phenomenological model for film transportation process on the wall

Figure 19   Boiling curve of each composition in an engine condition

and reflected droplets, shearing force of atmospheric gas, and friction force between liquid film and wall. This enabled pseudo-modeling of liquid film flow by the movement, although the discretized liquid film was a rigid body without flow in itself[28, 32].

Model considering the degree of superheat on heat transfer surface on the wall

In general, many of commercially distributed fuels have multiple components, which vary from low-boiling point

Figure 20   Spray impingement model available for transient boiling and film boiling conditions

components to high-boiling point components. Therefore, the mode of boiling on solid-liquid interface at impingement of the spray on wall surface varies depending on the fuel components even when a certain wall temperature is assumed. When the wall surface temperature range for a certain small direct injection diesel engine and light oil is subjected, the degree of superheat on wall surface ΔT_{sat} has a very wide range of -208 to 278 K and various boiling modes from non-boiling region to film boiling region as shown in Figure 19. Incidentally, the experiments by Takeuchi, et al. on impingement of single liquid droplets against high-temperature wall showed that the liquid droplets after breakup are dispersed in radial direction without liquid film formation in transition boiling or film boiling while the broken droplets were blown upward with liquid film formation in nucleate boiling region[22]. Therefore, the model developed before was applicable to the nucleate boiling region but not on transition boiling or film boiling. A model that could be applied to the transition boiling and film boiling regions was thus developed as shown in Figure 20[33, 34]. This comprised of liquid droplet breakup model, liquid droplet reflection model and heat transfer model. As shown in Figure 21, its calculation results express the difference in boiling modes that cannot be calculated by KIVA-II original codes, or the fact that the vapor concentration on wall surface is lower in transition and film boiling modes than that of nucleate boiling conditions as the droplets disperse without forming liquid film.
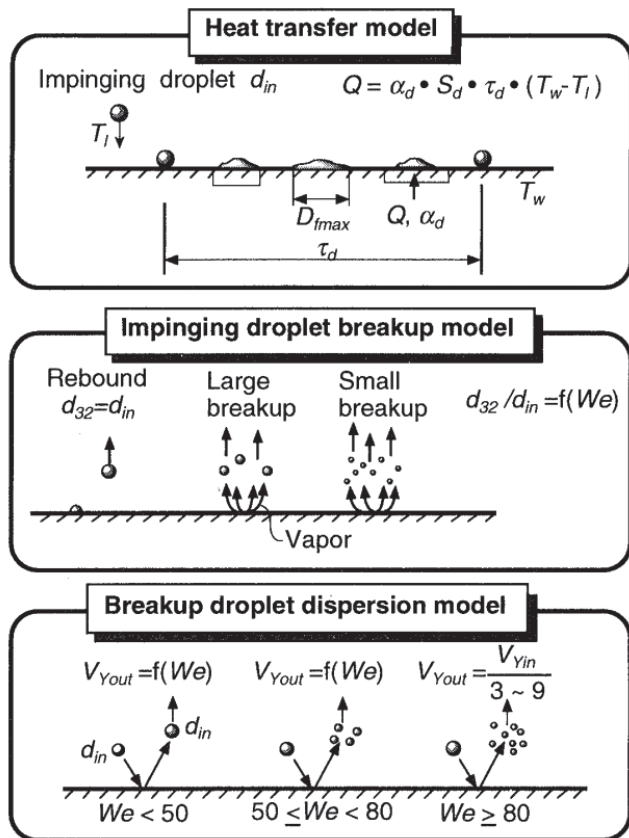
Model for expansion and integration in direct injection gasoline engines

While the models in the past had invoked the results of experiments on water droplet impingement on wall as the database on breakup and dispersion process after spray impingement, the wettability varies between water droplets and those of light oil or gasoline. Therefore, we prepared a database by conducting experiments on fine droplets by using 1-propanol (C_3H_8O) whose wettability was close to that of gasoline and whose boiling point was at 50% distillation temperature for gasoline as the liquid tested. It is also necessary that formation of liquid film and droplet dispersion and scattering be described for a wide range of wall surface temperature from low to high temperatures since light oil as well as gasoline are multi-component fuel. The authors therefore developed an integrated model applicable to all boiling regions with reference to the models that were developed in the past[35]. Its flow chart is shown in Figure 22. This model calculates the boiling region when a droplet impinges based on the saturated temperature for the fuel impinging on the wall surface and the wall temperature. They are

(a) Original model

(b) Nucleate boiling state (ΔT_{sat} = 50 [deg.])

(c) Transition boiling state (ΔT_{sat} = 150 [deg.])

(d) Film boiling state (ΔT_{sat} = 250 [deg.])

Distribution of vapor concentration
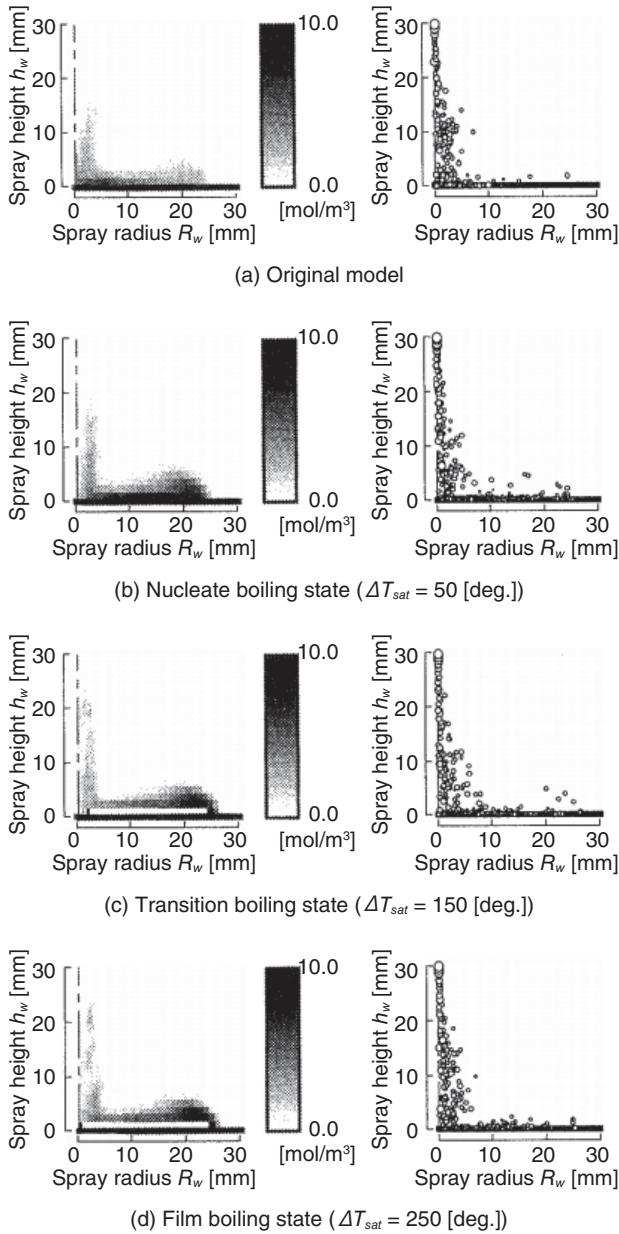
Distribution of droplet parcel

Figure 21　Comparison of spatial distribution of fuel vapor concentration and droplet parcels between KIVA-II original model and developed impingement model

Figure 22　Flowchart of integrated model

between droplets and so forth.

Modeling on Soot Particle Generation

Reduction of soot remains to be a great challenge in diesel engines and recent direct injection gasoline engines. Therefore, the authors developed a detailed chemical kinetic model to examine the soot generation and oxidation mechanism. As shown in **Figure 23**, this soot chemical kinetic model comprises of the following:

1) Gas phase reaction model which describes from fuel oxidation reaction, thermal decomposition to formation of aromatic ring, as well as growth of polycyclic aromatic hydrocarbon (PAH) up to heptacyclic, and

2) Soot particle generation model which describes condensation nucleus formation from PAH, agglomeration of particles, condensation of PAH

largely classified as low-temperature region and high-temperature region, and the dispersion rate, dispersion angle, droplet diameter and droplet temperature are calculated using the law of energy conservation and empirical equation based on experiment results on fine droplets as liquid film is not formed in high-temperature region. On the other hand, a model with consideration of interference among droplets and interference between liquid film and droplets is prepared to calculate the state of the droplets after breakup in low-temperature region where liquid film is formed. That is, it is calculated as a function of the angle of incidence, Weber number, degree of superheat on wall surface, liquid film thickness, gap
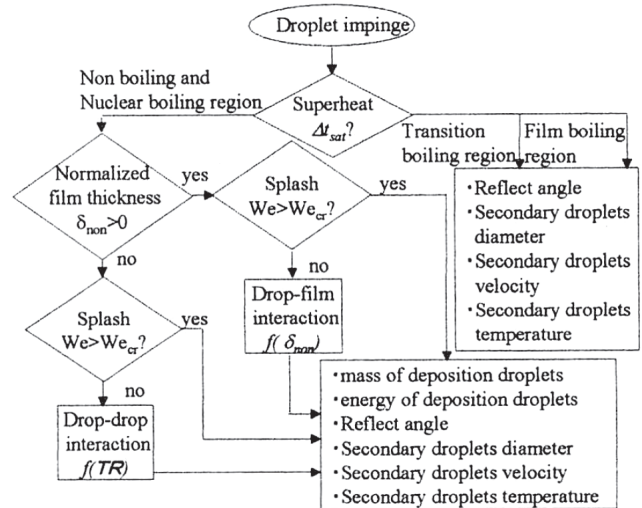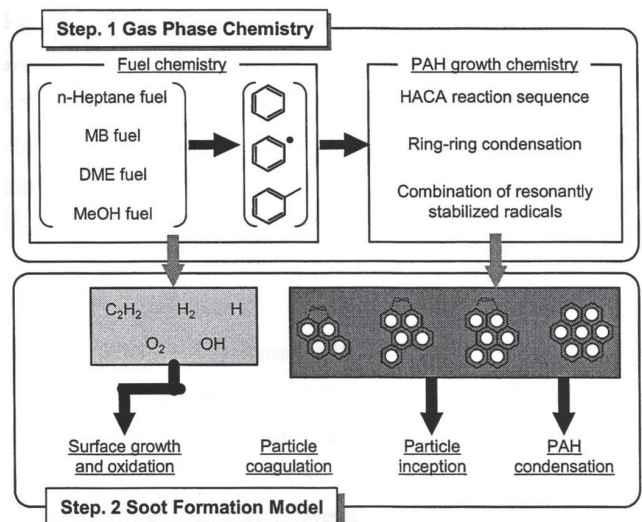

Figure 23　Reaction model for soot particle formation
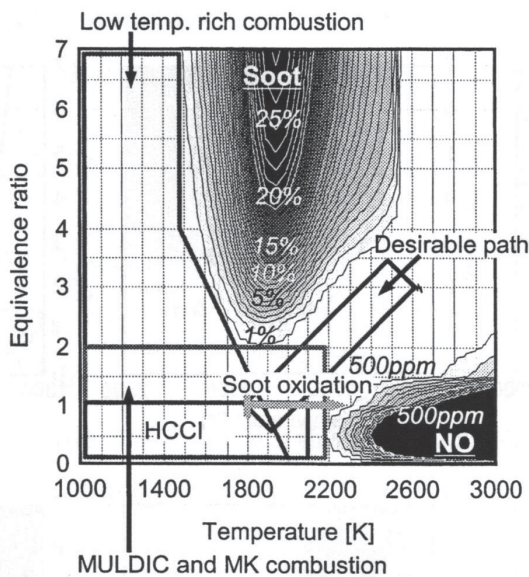
Figure 24 Comparison of representative diesel combustion methods on ø-T map (fuel: n-heptane, p=6MPa, reaction time: t=2ms)

ring (HACA mechanism) and binding reaction between aromatic rings were considered as the main reactions, with low-grade PAH generation reaction through binding between five-membered radicals also combined.

For the series of processes for PAH to be formed and grow to a primary soot particle as calculated in gas phase reaction, the following were taken into consideration:

1) "Nucleus generation process" to form a condensation nucleus from PAH,
2) "Condensation process" by collision and union of particles, and
3) "Surface growth process" by surface reaction between particle and gas phase chemical species and condensation of PAH on particle surface.

Please see Literature [38] for details about the above model.

on particle surface, and surface growth and oxidation reaction by gas phase chemical species.

The gas phase reaction model calculates the generation of PAH through thermal decomposition or oxidation, polymerization, cyclization and polycyclization reactions of the fuel molecules in gas phase using a detailed elementary reaction model as well as the concentrations of gas phase chemical species (PAH, C_2H_2, H_2, H, O_2, OH) that are necessary for calculation of the later-described particle nucleus generation and subsequent primary particle growth. We adopted the method using the mechanism by Apple and Bockhorn, Frenklach[37], which is an improved version of the mechanism by Wang and Frenklach[36] and combining a fuel oxidation reaction model with it. For polycyclization reaction from benzene (C_6H_6) to coronene (six-membered ring PAH: $C_{24}H_{12}$), PAH growth by hydrogen abstraction reaction on aromatic

Constant pressure-constant temperature fuel calculation was conducted using the developed model. Figure 24 shows the calculated soot generation yield and NO volumetric concentration on the ø-T map[39] proposed by Kamimoto, et al. (fuel: n-heptane: $n-C_7H_{16}$, pressure: 6 MPa). The figure also states the combustion conditions for typical clean diesel combustion method. It shows that the soot generation yield has a bell-shaped temperature dependency with a peak around 1900 K regardless of the equivalent ratio, and that the maximum value for soot generation yield increases as the equivalent ratio is higher. In addition, this figure indicated that the conventional soot reduction combustion methods are roughly classified into "temperature control types" to utilize the low-temperature size of the soot generation peninsula on the ø-T map and "equivalent ratio control types" to utilize the diluted fuel side. Figure 25 shows the soot particle diameter, number density and naphthalene as a soot precursor on the ø-T map. It was indicated that the soot
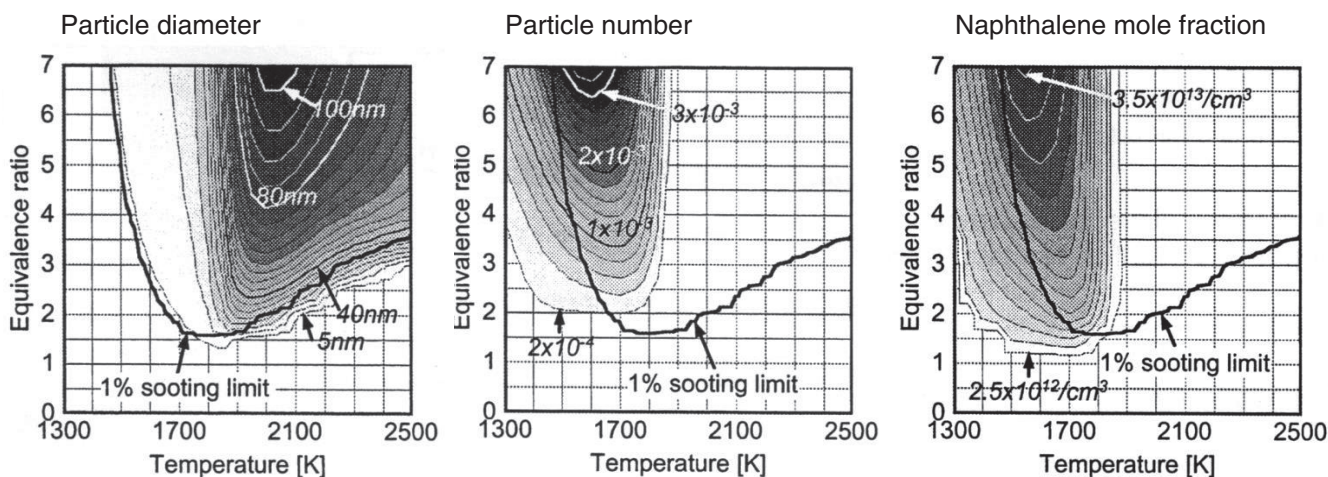

Figure 25 Distribution of particle diameter, particle number and naphthalene mole fraction on ø-T map (fuel: n-heptane, p=6MPa, reaction time: t=2ms)
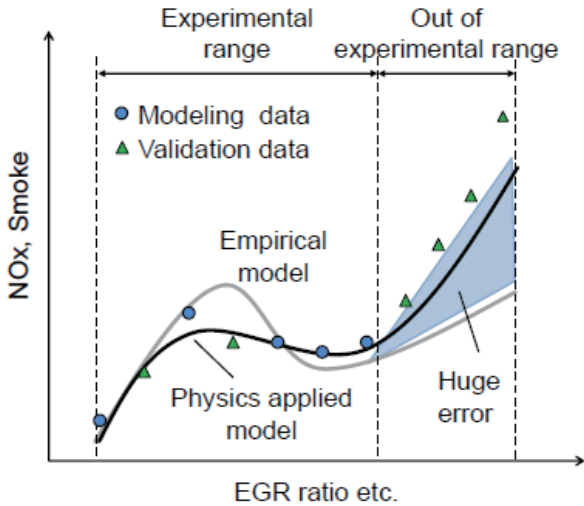
Figure 26 Advantage of applying physical theories into model based calibration
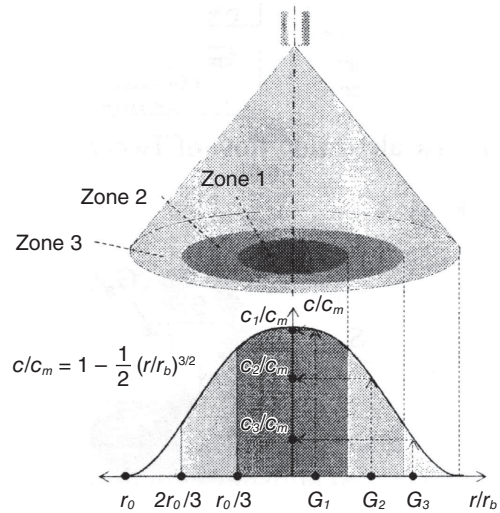

Figure 28 Distribution of fuel concentration divided into three zones in fuel spray

would be small in particle diameter, high in number density as well as PAH concentration in the range lower than the peak temperature of the bell-shaped soot generation yield, and that it would be large in particle diameter, low in number density and low PAH concentration in the range higher than the peak temperature.

Model Based Calibration with application of the laws of physics

At the end of this article, we introduce the development of

Figure 27 Flowchart of phenomenological model for model based calibration (MBC) method

Model Based Calibration (MBC)[40, 41], on which the authors have been working these days. MBC, which can develop an experiment model based on multivariate analysis on the minimum amount of actual measurement data and obtain the optimal design values using the model even against the recent increase in control parameters in engine development and concurrent exponential increase in man-hours for conformance experiments, has been under the spotlight. However, this method is not very precise when it is extrapolated outside the measurement range. The authors therefore have recently been trying to establish a model with which both interpolation and extrapolation are possible with high precision against the experiment range as shown in **Figure 26** by applying the laws of physics on an experimental model. The modeling flow chart is shown in **Figure 27**. The model comprises of spraying, combustion and emission models.
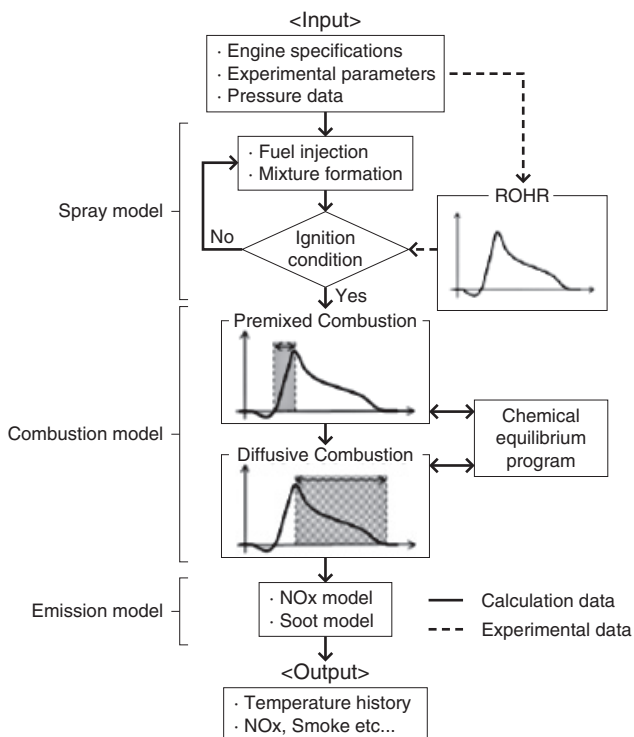
1) Spray model calculates the spray tip penetration, spray angle and breakup length using the equation by Hiroyasu[42] by dividing the space inside the cylinder into 2 regions of spray and atmosphere. In addition, the effect in which the spray velocity attenuates due to air resistance was considered after completion of injection. With supposition that introduction of air into the spray is started after the breakup length, and the theory of momentum by Wakuri[43] was used for its calculation. In addition, the distribution of fuel concentration in the radial direction of spray was calculated by supposing the law of three by two power which is a gas jet stream theory as shown in **Figure 28** to calculate as follows:

$$c/c_m = 1 - 1/2 \ (r/r_b)^{3/2} \quad \cdots\cdots\cdots\cdots\cdots\cdots\cdots \quad (17)$$
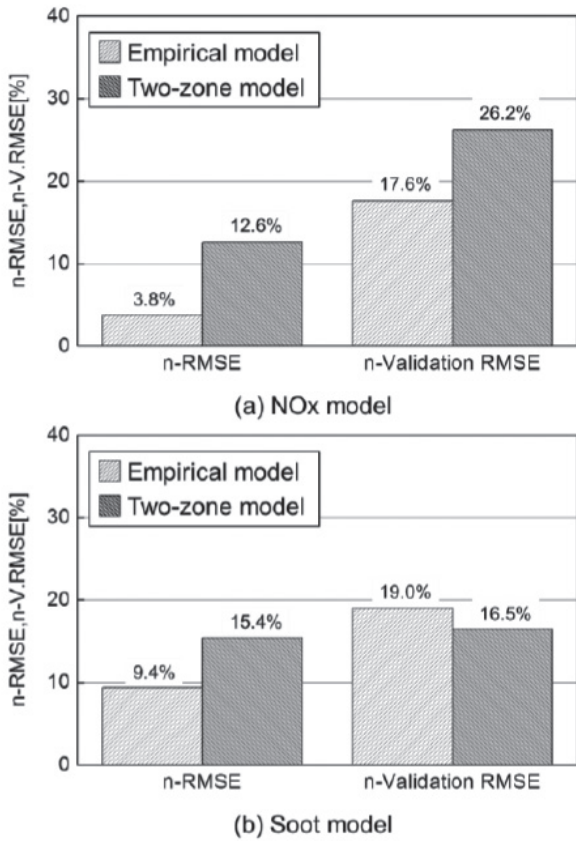
Figure 29   Example of evaluation results for NO$_x$ and soot models

(c: Fuel concentration in radial direction, c_m: fuel concentration on central axis for the spray, r: distance in radial direction, r_b: half-value width = $2/3r_0$, however, r_0 indicates spray outer periphery)
The spray area was further divided into 3 parts and was taken into consideration in the later combustion model.

2) Combustion model considers chemical equilibrium calculation among 10 chemical species in addition to the combustion reaction by hydrocarbons. The adiabatic flame temperature is calculated by enthalpy balance method during chemical equilibrium calculation.

The pattern for heat release rate was divided into premixed combustion period and mixing-controlled combustion period. One area close to the stoichiometric mixture in the 3 areas with different equivalent ratios within the spray burns during the premixed combustion period, and combustion reactions progress in all areas whose equivalent ratio values range from 0.5 to 3 during the mixing-controlled combustion period.

3) NO$_x$ and soot were considered subject in emission model. For NOx generation, expanded Zeldovich

mechanism was adopted with consideration of only the thermal NO. However, the equation below was used as the NO generation rate formula by replacing the constants with empirical constants α and β:

$$d\,[NO]\,/\,dt = \alpha\,[O_2]^{1/2}\,\exp\,(-\beta/T) \quad \cdots\cdots\cdots\cdots (18)$$

Here, T indicates the maximum average cylinder temperature and $[O_2]$ the oxygen concentration in cylinder and these are the main factors.

Hiroyasu model[44] was adopted as the soot model, and the soot oxidation reaction rate was described by the soot oxidation model[45] by Nagle, et al. The main factors were set as maximum average cylinder pressure, maximum average cylinder temperature, and molar fraction for oxygen molecules and it was modeled to include the empirical constants.

An example of calculation results on NO$_x$ and soot is shown in Figure 29. In addition, n-RMSE (normalized Root Mean Square Error) in the figure is an indicator obtained by normalizing the root-mean-square error between the model and the measurement data used for model preparation by the maximum and minimum values of the evaluation data. In addition, n-V. RMSE (normalized Validation RMSE) is an indicator obtained by normalizing the root-man-square error between the model and verification data by the maximum and minimum values of the evaluation data. It can be considered that the precision is appropriate with either of them being smaller than 10%. It is expected that the developed model can further be improved, although its precision is still lower than the empirical model except for the n-V. RMSE for soot. We have also been working on construction of a multicomponent fuel model applicable to MBC. The details are described based on the conceptual diagram in Figure 30. The spray tip penetration is calculated as follows according to the theory of momentum by Wakuri[43]:

$$x = \sqrt[4]{\frac{\rho_f}{\rho_a}} \cdot \sqrt{\frac{d_n u_0}{\tan\theta}} \cdot \sqrt{t} \quad \cdots\cdots\cdots\cdots (19)$$

(ρ_f: Fuel density, ρ_a: atmosphere density, d_n: nozzle diameter, θ: half-value for spray angle, t: time after injection start, u_0: injection velocity)
The mass of air introduced to the entire spray is calculated as follows:

$$M_E = \rho_a \cdot V_E = \frac{1}{3}\pi \cdot \rho_a \cdot \tan^2\theta \cdot x^3 \quad \cdots\cdots\cdots (20)$$
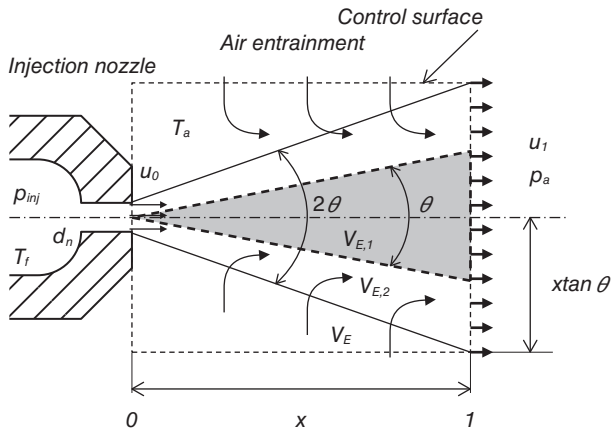
(M_E: Mass for introduced air, V_E: volume for

Figure 30   Schematic diagram of spray model used for 1-D multi-component spray model

Figure 31   Normalized liquid length and ignition delay calculated by 1-D multi-component fuel model

introduced air)

As shown in **Figure 30**, when spray area is classified, the cumulative mass of air introduced in each area is calculated as follows:

$$M_{E,1} = \rho_a \cdot V_{E,1} = \frac{1}{3} \pi \cdot \rho_a \cdot \tan^2 \left(\frac{\theta}{2} \right) \cdot x^3 \quad \cdots \cdots \quad (21)$$

$$M_{E,2} = M_E - M_{E,1} = \rho_a (V_E - V_{E,1}) \quad \cdots \cdots \cdots \cdots \quad (22)$$

In addition, subscripts 1 and 2 indicate the spray center and periphery, respectively. Therefore, the quantity of heat supplied to the fuel at time $n\Delta t$ after fuel injection start is expressed by the following equations:

$$\Delta Q_a = C_{p,a} \cdot \Delta M_{E,m,n} \cdot (T_a - T_e) \quad \cdots \cdots \cdots \cdots \cdots \quad (23)$$

$$\Delta M_{E,m,n} = \frac{1}{3} \pi \cdot \rho_a \cdot \tan^2 \theta \cdot (x_n^3 - x_{n-1}^3) \quad \cdots \cdots \quad (24)$$

($C_{p,a}$: specific heat of ambient gas at constant pressure, T_a: atmospheric temperature, m: spray center or periphery, T_e: equilibrium temperature)

Equilibrium temperature T_e is calculated implicitly with comparison to the fuel temperature calculated by SUPERTRAPP code[17] by supposing that the entire heat quantity supplied is consumed for fuel enthalpy increase. In addition, fuel composition is updated by simultaneously calculating the vapor-liquid equilibrium composition and physical property values for the fuel at the same time.

Livengood-Wu integration is adopted for calculation of ignition delay period.

$$X = \int_{t=0}^{t=n\Delta t} \left(\frac{1}{\tau_n} \right) dt \quad \cdots \cdots \cdots \cdots \cdots \cdots \cdots \cdots \cdots \quad (25)$$

Here, for instance, τ_n for n-dodecane (n-C$_{12}$H$_{26}$) is expressed by the following equation[46]:

$$\tau_n = 0.845 \times p_{amb}^{-1.31} \times \varnothing_{H.I.F}^{-1.60} \times \exp (4350/T_e) \quad \cdots \cdots \quad (26)$$

(p_{amb}: Atmospheric pressure, $\varnothing_{H.I.F}$: equivalent ratio for high self-ignition fuel)

The point when X exceeds 1 in **Equation 25** is considered to be the ignition. An example of calculation results is shown in **Figure 31**. This corresponds to the mixture of n-C$_5$H$_{12}$ and n-C$_{13}$H$_{28}$, and molar fraction for n-C$_5$H$_{12}$ is plotted on the horizontal axis. While the vertical axis is normalized so that only qualitative tendency is compared as the conditions such as atmospheric pressure varies, changes in liquid phase length against the mixture ratio, tendency for the ignition delay period to strongly depend on the high self-ignition component (n-C$_{13}$H$_{28}$ here) and so forth can be expressed.

Conclusion

As described in the beginning, development schemes that frequently use computers including development of model bases are being established in recent processes of engine development, and appearance of a simpler numerical model with higher precision is demanded for spray combustion. Thus this article described the important phenomena focused in development of models for various spray combustion processes the authors worked on and the methods of numerical model development. The numerical model for spray combustion is still under development. We hope that the information provided here would help advance the development.

References

[1] Y. Harada, *SEC journal*, **8-2**, 79-84 (2012)

[2] T. Kitada, M. Kuchida, S. Hayashi, *Journal of the Japan Institute of Marine Engineering*, **48-5**, 63-69 (2013)

[3] S. Oho, T. Aono, K. Suzuki, Y. Katsu, *Hitachi Review*, **91-10**, 54-57 (2009)

[4] W. Bergwerk: Proc. *Instn. Mech. Engrs.*, **173-25**,655-660 (1959)

[5] A. Shima, Y. Tomita, *Sokken report*, **34-334**, 125-161 (1974)

[6] Y. Wada, J. Senda, *Transactions of the JSME (in Japanese) B*, **72-724**, 3113-3120 (2006)

[7] K. Y. Huh and A. D. Gosman: *Proc. The International Conf. Multiphase Flows*, **'91-Tsukuba**, 515-518 (1991)

[8] P. J. O'Rourke and A. A. Amsden: *SAE Paper No.872089* (1987)

[9] J. Senda, T. Dan, S. Takagishi, T. Kanda and H. Fujimoto: *Proc. ICLASS-97*, 149-156 (1997)

[10] G. Stiesch: Modeling Engine Spray and Combustion Processes (Springer, 2003)

[11] J. C. Beale and R. D. Reitz: *Atomization and Sprays*, **9 (6)**, 623-650 (1999)

[12] R. D. Reitz: *Atomization and Spray Technology*, **3**, 309-337 (1987)

[13] K. Kitaguchi, S. Hatori, T. Hori and J. Senda: *Atomization and Sprays*, **22 (1)**, 57-77 (2012)

[14] T. Hori, T. Kuge, J. Senda, H. Fujimoto, *Transactions of the JSME (in Japanese) 2*, **73-727**, 879-886 (2007)

[15] J. Senda, Y. Ohta, T. Yamamoto, H. Fujimoto, *Transactions of the JSME (in Japanese) B*, **62-600**, 3205-3212 (1996)

[16] A. A. Amsden: Los Alamos National Laboratory Report LA-13313-MS (1997)

[17] National Institute for Standards and Technology, http://www.nist.gov/srd/nist4.cfm (accessed January 21, 2014)

[18] D. Kawano, J. Senda, Y. Wada, H. Fujimoto, Y. Ishii, Y. Suzuki, Y. Goto, *Transactions of the JSME (in Japanese) B*, **70-696**, 2213-2219 (2004)

[19] E. W. Curtis, A. Uludogan and R. D. Reitz: *SAE Paper No.952431* (1995)

[20] Y. Kobashi, K. Fujimori, H. Maekawa, S. Kato, D. Kawano, J. Senda, *Journal of Automotive Engineering (in Japanese)*, **43-1**, 123-128 (2012)

[21] M. P. Halstead, L. J. Kirsch and C. P. Quinn: *Combustion and Flame*, **30**, 45-60 (1977)

[22] K. Takeuchi, J. Senda, Y. Sato, **21-268**, 9-18 (1982)

[23] J. Senda, Ko. Yamada, K. Takeuchi, H. Miki, *Transactions of the JSME (in Japanese) B*, 53-485, pp.176-182 (1987)

[24] J. Senda, M. Kobayashi, S. Iwashita, H. Fujimoto, *Transactions of the JSME (in Japanese) B*, **60-578**, 3563-3570 (1994)

[25] J. Senda, M. Kobayashi, S. Iwashita and H. Fujimoto: *SAE Paper No.941894* (1994)

[26] J. Senda, T. Kanda, M. Al-Roub, P. V. Farrell, T. Fukami and H. Fujimoto: *SAE Paper No.970047* (1997)

[27] J. Senda, T. Kanda, S. Kusano, H. Fujimoto, *Transactions of the JSME (in Japanese) B*, **65-629**, 389-396 (1999)

[28] A. Utsunomiya, M. Ohnishi, J. Senda, H. Fujimoto, *Transactions of the JSME (in Japanese) B*, **65-629**, 397-402 (1999)

[29] M. A. Al-Roub, P. V. Farrell and J. Senda: *SAE Paper No.960863* (1996)

[30] M. A. Al-Roub: Ph.D. Thesis at Univ. of Wisconsin-Madison (1995)

[31] J. D. Naber and R. D. Reitz: *SAE Paper 880107* (1988)

[32] J. Senda, M. Onishi, T. Takahashi, H. Fujimoto, A. Utsunomiya and M. Wakatabe: *SAE Paper No. 1999-01-0798* (1999)

[33] J. Senda, T. Takahashi, T. Tanaka, J. Li, H. Fujimoto, *Transactions of the JSME (in Japanese) B*, **66-642**, 604-611 (2000)

[34] J. Senda and H. Fujimoto: *SAE Paper No.2001-01-1071* (2001)

[35] K. Matsuda, J. Senda, H. Fujimoto, 11th ILASS-Japan, 26-31 (2002)

[36] H. Wang and M. Frenklach: *Combustion and Flame*, **110**, 173-221 (1997)

[37] J. Appel, H. Bockhorn and M. Frenklach: *Combustion and Flame*, **121**, 122-136 (2000)

[38] T. Kitamura, T. Ito, J. Senda and H. Fujimoto: *International Journal of Engine Research*, **3-4**, 223-248 (2002)

[39] T. Kamimoto and M. H. Bae: *SAE Paper No. 880423* (1988)

[40] M. Okamoto, Y. Tanaka, Y. Shimizu, M. Matsumoto, J. Senda, Y. Kitamura, H.Yuasa, A. Kato, *Journal of Automotive Engineering (in Japanese)*, **44-2**, 245-250 (2013)

[41] K. Akihisa, M. Okamoto, M. Matsumoto, E. Matsumura, J. Senda, Y. Kitamura, M. Sato, H.Yuasa, A. Kato, *Journal of Automotive Engineering (in Japanese), No.72-20135683* (2013)

[42] H. Hiroyasu, M. Arai, *Journal of Automotive Engineering (in Japanese)*, **21**, 5-11 (1980)

[43] Y. Wakuri, T. Amiya, R. Tsuneya, *Transactions of the JSME (in Japanese) 2*, **25-156**, 820-826 (1959)

[44] K. Nishida and H. Hiroyasu: *SAE Paper No. 890269* (1989)

[45] J. Nagle and R. F. Strickland-Constable: *Proc. 5th Carbon Conference*, 154-164 (1962)

[46] S. Ikura, et al., *Transactions of the JSME (in Japanese) 2*, **41-345**, 1559-1568 (1975)